

TUNNELING MICROSCOPY AND SPECTROSCOPYL. J. WHITMAN, *Naval Research Laboratory, Washington, DC 20375-5342*

Introduction	1	3.3 Electrochemistry	15
1. Microscope Components ...	3	3.4 Surface Electronic Structure ...	16
1.1 Scanner	3	3.4.1 Conductance versus Structure	16
1.2 Coarse Approach	4	3.4.2 Chemically-Selective Imaging	17
1.3 Vibration Isolation	5	3.5 Bulk Electronic Structure ...	17
1.4 Control Electronics	5	3.6 Atom Manipulation and Nanolithography	18
1.5 Tip Preparation	6	3.6.1 Electron-Stimulated Patterning	19
2. Principles of Imaging and Spectroscopy	6	3.6.2 Positioning Single Atoms ...	19
2.1 Tunneling Physics	6	4. Related Techniques	20
2.2 Density of States Effects	7	Acknowledgments	21
2.3 Imaging Modes	8	Glossary	21
2.4 Tunneling Spectroscopy	8	Works Cited	22
3. Applications	9	Further Reading	23
3.1 Structure of Crystal Surfaces .	10		
3.1.1 Metals	10		
3.1.2 Semiconductors	11		
3.1.3 Oxides	12		
3.2 Adsorption and Film Growth .	12		
3.2.1 Atom-Resolved Surface Chemistry	13		
3.2.2 Thin-Film Morphology	14		

INTRODUCTION

Scanning tunneling microscopy (STM) is a laboratory technique capable of obtaining atomic-scale resolution images of surfaces. It can also be used for tunneling spectroscopy measurements that reveal a variety of surface electronic properties with similar spatial resolution. Moreover, under appropriately controlled conditions an STM can be used to move individual surface atoms and molecules with atomic-scale precision. For such a powerful instrument, the basic operating principles are remarkably

simple. As illustrated in Fig. 1, a sharp metal tip is brought within 1 nm of the surface of an electrically-conductive sample and a few volts are applied between the two, enabling electrons to quantum-mechanically tunnel across the tip-surface gap. The resulting tunnel current, typically on the order of 1 nA, depends exponentially on the gap: a change of 0.1 nm causes the current to change by a factor of ~10, giving STM atomic-scale sensitivity. If the gap is regulated to keep the current constant while the tip is scanned laterally, adjacent profiles

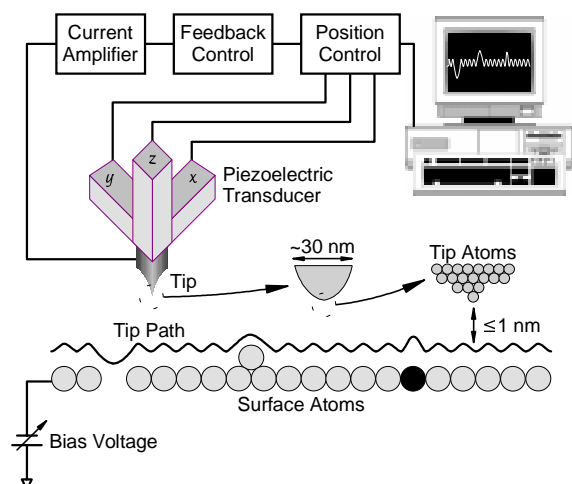


FIG. 1. The basic elements of scanning tunneling microscopy.

of the surface topography can be assembled into an image via computer. As shown in Fig. 2, images of the surface topography can then be displayed in gray-scale (with high points brighter) or artificially rendered as a 3D surface (usually with exaggerated height).

STM has its origins in the “topografiner” developed in the early 1970’s (Young *et al.*, 1972), that included most of the elements of an STM but operated with a larger tip-to-surface gap (>1 nm, at which distance electron transport occurs via field emission). Deficiencies in both the mechanical and electrical systems at that time limited the resolution to a few nanometers vertically and ~ 0.5 μm laterally. These problems were overcome about ten years later by Gerd Binnig and Heinrich Rohrer at the IBM R schlikon laboratory, who succeeded in creating an instrument with stable vacuum tunneling and precision scanning capabilities – the conditions required for atomic resolution imaging – for which they were awarded the 1986 Nobel Prize in physics (Binnig *et al.*, 1982a; Binnig *et al.*, 1982b). STM has revolutionized the study of surfaces and is rapidly becoming a required tool in every surface characterization

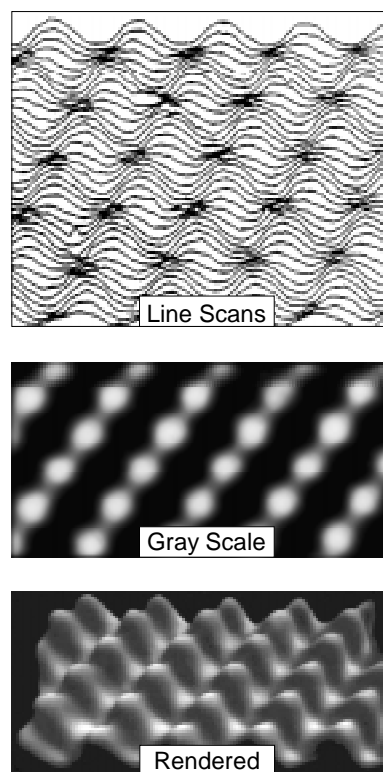


FIG. 2. Three common ways of presenting an STM image: as a set of line scans; in gray scale, with higher points brighter; and as an artificially-rendered surface.

laboratory. In addition, it has led to the development of a host of related techniques, collectively known as scanning probe microscopies, and spawned an industry aimed at providing reliable, easy-to-use commercial instruments.

Given the many comprehensive books and review articles about STM that are available (see Further Reading), only the experimental details and theoretical concepts essential for a general understanding of the operation and application of STM are presented here. The technical components of the microscope are discussed first, followed by the theoretical principles of operation. Applications are then presented that illustrate the capabilities and limitations of STM under optimal conditions. Lastly, some related techniques are discussed.

1. MICROSCOPE COMPONENTS

To achieve atomic-scale resolution, the mechanical and electrical components of an STM must enable the tip to be positioned within approximately 1 nm of the surface and then controlled both vertically and laterally with a precision of <0.01 nm. This precision requires low-vibration mechanical systems combined with low-noise electrical circuitry. Myriad ways have been developed to achieve the required mechanical stability; the more common elements are illustrated in Fig. 3. The STM must include a coarse approach mechanism, such as the “inchworm” motor shown, capable of bringing the tip into tunneling range with the sample. Once in range, a scanning transducer controls the vertical and lateral position of the tip over the sample. The sample and scanner are mounted in a rigid framework to minimize the effect of mechanical resonances. A vibration isolation system, often based on a magnetically-damped spring suspension, is usually required to reduce transmission of external vibrations. Photographs of a complete ultra-high vacuum (UHV)-based system is shown in Fig. 4, including the UHV system required to maintain a pristine sample surface.

1.1 Scanner

The position transducer is the central element of the STM, and is almost universally composed of the piezoelectric ceramic PZT [$\text{Pb}(\text{Zr},\text{Ti})\text{O}_3$]. This material expands or contracts approximately linearly with the voltage applied across it (see PIEZOELECTRIC DEVICES). Although early STM designs used a tripod of three orthogonal bars to control motion in three dimensions, a tube geometry is more common now due to its inherent rigidity. The design of a typical tube scanner is shown in Fig. 5 (Binnig and Smith, 1986).

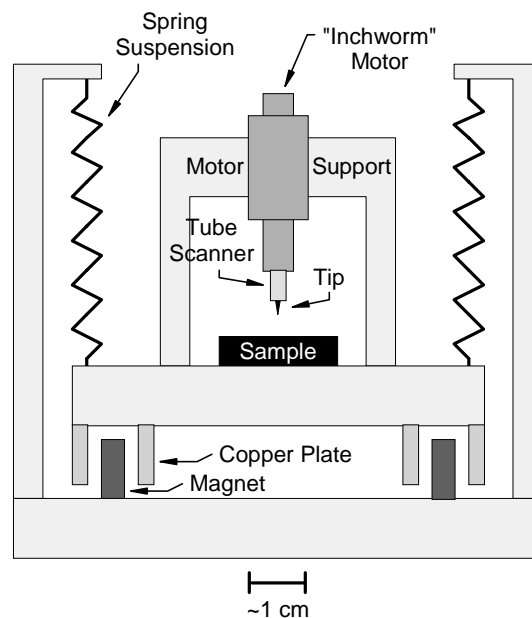


FIG. 3. Common elements of an STM, including a tip mounted on a piezoelectric tube scanner, a coarse approach mechanism (in this case an “inchworm” motor), and a damped vibration isolation system.

A thin-walled tube of PZT is coated with metal on the inner and outer surfaces, with the outer surface divided into four equal quadrants by narrow metal-free regions. The inner surface is then used as the electrode for the vertical displacement (z), and the opposing pairs of outer electrodes are used for lateral motion (x and y). In this geometry a voltage applied between the inner and outer electrodes causes the tube to change length. Opposite voltages applied across opposing outer electrodes will induce one side of the tube to contract and the other to expand, causing a net lateral displacement (along with a small vertical displacement that can usually be ignored). For example, a 15 mm-long, 2.5 mm-radius, 0.75 mm-thick tube of a common commercial PZT material driven by voltages between +150 and -150 V would provide an overall scan range of $1.0 \mu\text{m}$ vertically and $2.8 \mu\text{m}$ laterally.

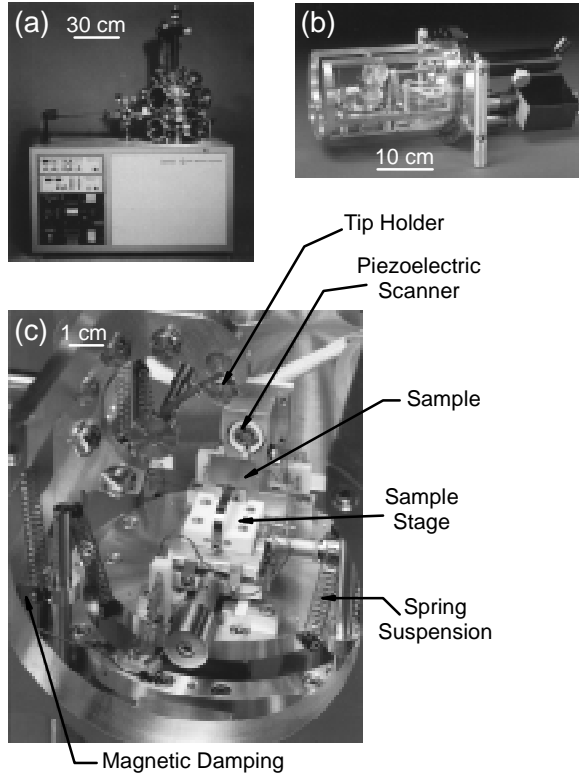


FIG. 4. Photographs of a commercially available STM (AutoProbe® VP, Park Scientific Instruments, Sunnyvale, CA). (a) Complete ultra-high vacuum system. (b) STM mounted on vacuum flange. (c) close up of STM showing the tip holder being transferred to the scanner.

1.2 Coarse Approach

The tip-surface gap can usually be reduced to <0.1 mm via optical inspection. The basic requirement of the subsequent coarse approach is that the remaining gap be reduced in steps less than the z -deflection range of the piezotube. This requirement allows a step to occur with the piezotube retracted, followed by a controlled expansion towards the surface (in a search for tunneling), without crashing the tip into the surface. Myriad ways have been developed to achieve this result. Two common techniques, the “inchworm” motor and the inertial slider, are depicted in Fig. 6.

In an inchworm motor [Fig. 6(a)], a shaft is clamped inside a piezotube by additional piezoelectric material. If the position of the outer tube is fixed at one point, an

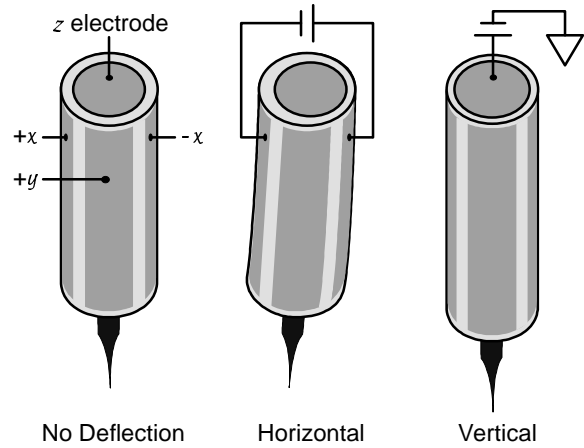


FIG. 5. Operation of a piezoelectric tube scanner with a four-quadrant outer electrode for horizontal motion and single inner electrode for vertical motion. A horizontal deflection occurs when a voltage is applied across opposing outer electrodes. A vertical deflection occurs when a voltage is applied to the inner electrode with respect to the four outer electrodes.

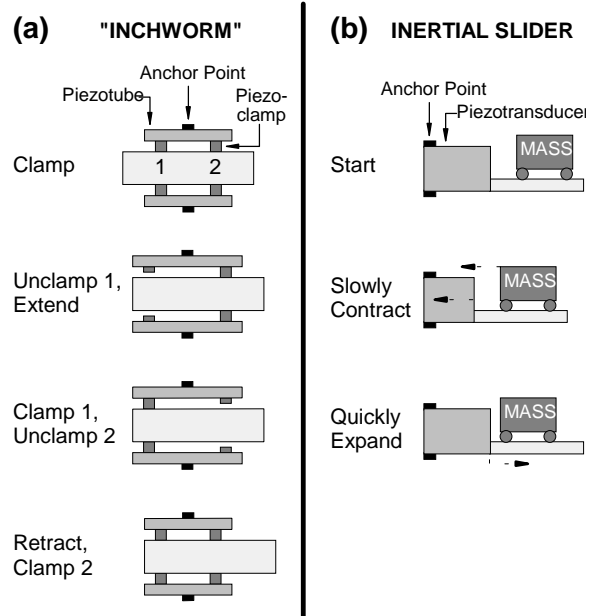


FIG. 6. Operating principles for two common coarse approach mechanisms. (a) An “inchworm” motor employs a piezotube and piezoclamps to move an inner shaft with a series of clamping/unclamping and extension/retraction events. (b) Inertial motion of a free mass can be achieved by asymmetrical acceleration.

inchworm-like series of clamping-unclamping and extension-retraction events will move the shaft. For simplicity, a tube scanner and tip can be mounted directly onto the end of an inchworm shaft (as in Fig. 3). Alternatively, an inchworm-like device can be used to push/pull the sample or scanner along a sliding mechanism.

Inertial motion uses asymmetrical acceleration to induce asymmetrical stick-slip motion of a mass. For example [Fig. 6(b)], if the transducer is first contracted slowly enough to prevent sliding, the mass will move with it; if the transducer is then expanded rapidly enough to induce sliding between the mass and its contact with the transducer, the mass will remain in place during the expansion, thereby effecting a net movement towards the anchor point. A variety of implementations of this strategy have been developed, with the tip, scanner, or sample stage acting as the mass.

1.3 Vibration Isolation

The amplitude of any vibrations between the tip and surface must be reduced as much as possible to achieve optimum resolution. To achieve atomic-scale resolution the noise must be well below 0.01 nm within the frequency response of the tunneling control system (typically ~ 10 kHz). Because the amplitude of floor vibrations and other acoustic noise in this frequency range typically ranges from 0.1 to 1 μm , this is a considerable challenge. The transmission of these vibrations can be reduced by making the components of the STM as rigid as possible, especially those in the mechanical loop between the tip and sample, and mounting the scanner-plus-sample assembly on a vibration isolation stage. There are two basic approaches to vibration isolation. The first involves suspending the assembly from one or more sets of springs with resonant frequencies of a few Hertz. Because a

spring suspension has little inherent damping (it will easily oscillate at its resonant frequency), external damping is usually added in the form of permanent magnets suspended between copper plates (see Fig. 3). So called eddy-current damping works by electromagnetically inhibiting the relative motion between the magnets and the high-conductivity metal plates. The second approach to vibration isolation is to mount the instrument on a stack of heavy metal plates separated by rubber-like spacers. Although this approach is generally less effective than a spring system, it is easier to build and simpler to operate.

1.4 Control Electronics

The essential elements of the control electronics, as included in Fig. 1, are: a current amplifier; a feedback control system; a position control system, including digital-to-analog converters (DAC), analog-to-digital converters (ADC), and high-voltage amplifiers to control the scanner; and a computer for overall program control and image display. The tunneling current is typically in the range of 0.1 to 10 nA, and to keep it constant via feedback it is usually converted to a reference voltage ~ 1 V; this requires a current-to-voltage amplifier with a gain of 10^8 to 10^{10} V/A and noise below the equivalent of 10 pA (readily achievable with commercial electronic components). Because the current varies exponentially with the tunneling gap, an amplifier that converts the input signal to its logarithm is usually employed between the current-to-voltage amplifier and the feedback in order to linearize the system response. Proportional and/or integral feedback is used to generate a voltage to control the height of the tip above the surface. Because this voltage represents the surface topography, it is sent to the ADC for storage and display. The main function of the position control

system is to convert the computer-generated low-voltage DAC signals into the appropriate high-voltage signals for control of the scanner position. To record a topography image, the tip is scanned back and forth across a surface area, taking small steps perpendicular to each scan line, while periodically recording the tip height. The result is a two-dimensional array of height values that can be displayed as an image (see Fig. 2.).

1.5 Tip Preparation

The tunneling tip is the most critical component of the STM, as it ultimately determines the resolution and overall image quality. Both the shape of the tip and the types of atoms on the end affect the images; in the ideal case, tunneling occurs through a single atom at the apex of a microscopically sharp metallic tip. As the number of atoms on the apex of the tip increases, the resolution degrades, although atomic resolution can still be achieved with a cluster of a few atoms. If the surface being studied is very flat (on the nanometer scale), only the atomic-scale shape of the tip apex is important, because only those atoms near the end will contribute to tunneling. In contrast, on rougher surfaces the recorded topography may be a noticeable convolution of the surface topography and the microscopic tip shape. Because the tunneling current depends not only on the gap but on the electronic structure of the tip as well (see Section 2), a nonmetallic atom or cluster on the tip apex may also affect the image.

The most common materials used for tips are tungsten and platinum-iridium alloy wires. Although good resolution can sometimes be obtained using a crudely cut wire – when nature conveniently leaves a single atom or small atom cluster on the jagged apex of the cut – more reproducible results are obtained with tips

electrochemically etched to a sharp point. Pt-Ir is often used for tunneling in air due to its resistance to oxidation; W is preferred for UHV applications, in part due to the knowledge gained about its preparation for use in field ion microscopy (FIM; see FIELD ION MICROSCOPY). W tips can be easily etched to a microscopic radius of <10 nm and, fortunately, it is not uncommon for there to be an atomic-scale cluster on the end as required for atomic-scale resolution.

2. PRINCIPLES OF IMAGING AND SPECTROSCOPY

The inherent resolution of STM is a direct consequence of the quantum mechanical tunneling between the tip and surface. This current depends both on the width and height of the tunneling barrier, and on the electronic structure of the tip and surface. By measuring the interdependence of the various tunneling parameters, e.g. bias voltage, tunneling current, and tunneling gap, images and spectra of a variety of surface electronic properties can be recorded in addition to topography. In this section, an overview of the essential physics of these processes is provided.

2.1 Tunneling Physics

Figure 7(a) illustrates an idealized potential energy diagram for the electrons in a metal sample and tip a distance s apart, with work functions ϕ_s and ϕ_t , respectively, and a positive bias voltage V applied to the sample. In a classical picture, the work function, which is the energy required to move an electron at the surface from the Fermi level (E_f) to the vacuum, prevents electron transport between the two electrodes. Quantum mechanical tunneling, however, can occur due to the overlap of electron wave functions that span the gap. If the potential energy barrier is treated as a simple trapezoid, the probability for an

electron on the tip at energy E with respect to E_f^t to tunnel to the surface can be approximated as

$$T \approx \exp \left\{ -2s \left[\frac{2m}{\hbar^2} \left(\bar{\phi} - E - \frac{eV}{2} \right) \right]^{\frac{1}{2}} \right\}, \quad (1)$$

where $\bar{\phi}$ is the average work function of the tip and sample, m is the electron mass, e is the electron charge, and \hbar is Planck's constant. For small bias voltages, the probability of tunneling for tip electrons near E_f^t can be further approximated as

$$T(s) \approx \exp(-2\kappa s), \quad (2)$$

where κ is the vacuum decay constant, $(2m\bar{\phi}/\hbar^2)^{1/2}$, about 10 nm^{-1} for typical work functions.

2.2 Density of States Effects

The net tunneling current depends on the total number of sample and tip surface electronic states that overlap within the energy range for which tunneling can occur, as schematically shown in Fig. 7(b). When a positive bias voltage is applied to the sample (or conversely, a negative voltage is applied to the tip), electrons in occupied states on the tip can elastically tunnel into the energy-equivalent empty states in the conduction band on the sample. Similarly, a negative sample bias allows electrons occupying filled states on the surface to tunnel into empty states on the tip. The probability for each of these tunneling events is given by Eq. (1). Mathematically, the net tunneling current can be approximated as:

$$I \propto \int_{-eV}^0 \rho_t(E) \rho_s(eV + E) T(E, eV) dE, \quad (3)$$

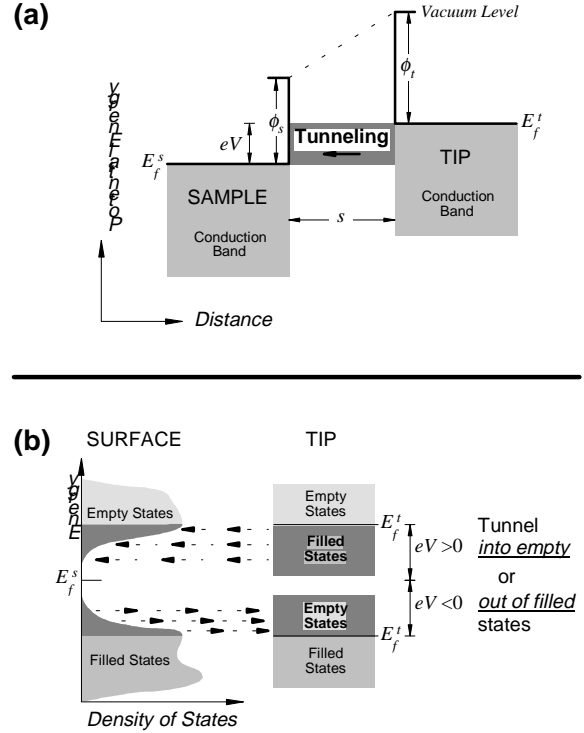


FIG. 7. (a) Schematic of quantum-mechanical tunneling between a metal tip and metal surface a distance s apart. The tunneling barrier is determined by the work functions of the surface and tip, ϕ_s and ϕ_t , respectively, and the bias voltage applied between the two, V . For the case shown, surface positive with respect to the tip, electrons tunnel from bands below the Fermi level of the tip to those above the Fermi level of the surface. (b) Detailed schematic of the role of the density of states near E_f on the tunneling process both into and out of empty and filled states, respectively, on a semiconductor surface.

where ρ_s and ρ_t are the energy-dependent density of states for the sample and tip, respectively. For metals (including the tip), ρ is approximately constant near the Fermi level, with states being uniformly filled below E_f and empty above. On semiconductor surfaces ρ may be a strongly-varying function of energy (possibly including energies where it is near zero as depicted in Fig. 7), thereby dominating the voltage dependence of the tunneling current.

2.3 Imaging Modes

The primary operational mode of STM is *constant current imaging*, where the height of the tip is recorded as it is rastered over the surface while the tunneling current is kept constant. When tunneling occurs from sample to tip, the result is a *filled-state* topographic image; tunneling from tip to sample provides an *empty-state* image. On a perfectly crystalline surface the corrugation of the topography from atom-to-atom (i.e. peak-to-valley height) typically ranges from 0.001 to 0.01 nm on metals and 0.01 to 0.1 nm on semiconductors. If the density of states is relatively uniform across a surface, and modulated only by the location of surface atoms (as is usually the case for metals), the topography will represent a simple contour of constant height of the tip above the surface atoms. Frequently, however, $\rho_s(E)$ varies across the surface from atom-to-atom, and at some energies may not even be a maximum over the atom cores. In such cases the images will look different at different bias voltages (the topographic maxima may even move), making interpretation difficult. The density of states dependence [Eq. (3)], leads to a central tenet of STM: *constant current topography measures (at best) the surface of constant integrated density of states, a surface that is generally bias-dependent and may not correlate with the positions of the surface atoms.* This tenet also reveals another limitation of STM: *it is not directly sensitive to the chemical identity of surface atoms.* Fortunately, by complementing topographic images with spectroscopic information (as described below) and the results of other surface characterization techniques, it is often possible to infer the chemical composition of a surface. Furthermore, these limitations chiefly affect atomic-resolution studies of single-crystal surfaces, and are not usually of consequence

when topography on the nanometer scale is of primary interest.

A second common method of acquiring STM images is known as *current imaging*. In this mode, images are acquired by recording the tunneling current while the tip is rastered at constant height. The result is an image of the variation of the integrated density of states at a fixed height above the surface atoms. This method can only be used on very flat surfaces where the roughness is less than the tunneling gap, but has the advantage of being very fast because only minimal feedback is required.

Another standard data acquisition mode is *multi-bias imaging*, where multiple constant current topographs are recorded simultaneously with different bias voltages. Such images, typically recorded by repeating each scan line at multiple biases before advancing to the next line, reveal the spatial and energy dependence of the integrated density of states at the surface, and are often useful for interpreting atomic-scale features. A number of examples can be found in Sec. 3.1 below.

2.4 Tunneling Spectroscopy

By measuring the dependence of the tunneling current on the tip-surface gap or the bias voltage, spectra containing information about the work function or density of states on the surface can be obtained. Furthermore, because tunneling only occurs over an area $<1 \text{ nm}^2$ on the surface, such spectra reveal these properties on an atomic scale. The average work function can be extracted by measuring I as a function of s at fixed V . From Eqs. (2) and (3) we find that

$$\bar{\phi} \approx \frac{\hbar^2}{8m} \left(\frac{d \ln I}{ds} \right)^2. \quad (4)$$

The I - s measurements, sometimes referred to as barrier height spectra, can be performed periodically over the surface to create an image of the average work function.

Scanning tunneling spectroscopy most often refers to a second type of measurement: the dependence of I on V at fixed s . This measurement is usually made by temporarily disabling the feedback, holding the tip in place, and ramping V while measuring I . I - V spectra reveal features of the local density of states on the surface, as expressed in Eq. (3). Because the exponential dependence of the tunneling probability on V [Eq. (2)] may conceal features in the spectra associated with variations of the density of states, the differential conductance, dI/dV , is often displayed instead of I . Neglecting any role of the tip density of states,

$$dI/dV \propto \rho_s(eV)T(eV). \quad (5)$$

The effects of $T(eV)$ can be further compensated for by normalizing dI/dV to the total conductance, I/V , revealing most clearly the features associated with the surface density of states:

$$\frac{dI/dV}{I/V} \propto \rho_s(eV). \quad (6)$$

I - V spectra can be made at every point in a topographic image to create a set of spectroscopy images that show the spatial variation of the density of states as a function of voltage. The interpretation of specific I - V spectral features is usually made by comparison with analogous photoemission and inverse photoemission spectra (see PHOTOEMISSION AND PHOTOELECTRON SPECTRA).

3. APPLICATIONS

One of the more remarkable aspects of STM is the wide range of environments in which it can operate: a stable tunnel current can be maintained in almost any non-conducting medium, including air, liquid, or vacuum. STM operation is also relatively forgiving when it comes to sample preparation: the main requirement is that the sample conduct ~ 1 nA at ~ 1 V. This flexibility allows a wide range of applications. Due to the inherent surface sensitivity of STM, it is most widely applied in the field of surface science – the study of the structural, electronic, and chemical properties of surfaces, interfaces, and thin films – a field important to a wide range of technologies, including catalysis, semiconductor device fabrication, electrochemistry, and chemical sensors. The technique is especially useful for elucidating the properties of nanometer-sized surface structures. The operating flexibility of STM combined with the ability to acquire spectroscopic images has also led to its application in the study of novel electronic properties of materials, such as charge density waves and superconductivity. Finally, the close proximity of the tip to the surface enables one to modify surfaces with atomic-scale precision.

Although STM images and spectra can be recorded under a variety of conditions, the sensitivity of the tunneling current to any perturbation, such as the adsorption of a contaminant atom or molecule on the tip or sample, or mechanical vibration, is such that the best results are obtained with carefully prepared tips and surfaces within the controlled environment of a UHV chamber, electrochemical cell, or helium-filled cryogenic refrigerator. With the aim of best illustrating the unique microscopic and spectroscopic capabilities of STM, most of

the applications chosen for this Section were obtained under such optimal conditions.

3.1 Structure of Crystal Surfaces

The surface of a crystal can be described by its “Miller indices,” (hkl). For a cubic crystal, the indices define a vector perpendicular to the surface in terms of the axes of the crystal lattice, $h\hat{x} + k\hat{y} + l\hat{z}$. For example, a (111) surface is perpendicular to the long diagonal of the cube. Due to the loss of three-dimensional periodicity on a surface, the exposed atoms on most crystal faces move from their bulk lattice positions, a rearrangement referred to as surface reconstruction. The reconstruction is described by additional notation, ($m \times n$), that refers to the size of the *unit cell*, which is the periodic structural unit on the surface, in relation to that of the bulk. For example, a (2×1) reconstruction on a cubic (001) surface would have a unit cell twice as large in the x -direction and of equal size in y as on the bulk-terminated surface.

The ability to obtain real-space, atomic-resolution images of single-crystal surfaces has revolutionized the study of surface structure, particularly on surfaces with complex unit cells or point defects. This advance has had a major impact in surface science because determining the structure of clean surfaces is the first step to understanding their electronic and chemical properties. Note that whereas on metal surfaces the interpretation of STM topography is relatively straightforward, on other surfaces it is often necessary to complement STM results with other surface characterization techniques or theoretical calculations to properly assign topographic features to surface structures.

3.1.1 Metals One of the more dramatic illustrations of surface reconstruction is the so-called “herringbone” ($23 \times \sqrt{3}$) structure

on Au(111), images of which are shown in Fig. 8. STM was instrumental in the determination of the complex structure of this large-scale reconstruction (Wöll *et al.*, 1989), which entails a contraction of the lattice at the surface such that there are 23 atoms for every 22 bulk-like lattice sites. This contraction creates a herringbone-like superstructure of partial dislocation ridges [raised areas in Fig. 8(a)] where surface atoms switch back and forth between their bulk positions [face-centered cubic (FCC) and hexagonal close-packed (HCP) lattice sites]. At each “knee” in the superstructure there is a surface dislocation (where the 23rd row of atoms ends), as seen with atomic-resolution in Fig. 8(b). This example highlights the extreme sensitivity of STM: the surface atoms, less than 0.3 nm apart, are visible as peaks in the topography only 3 pm high.

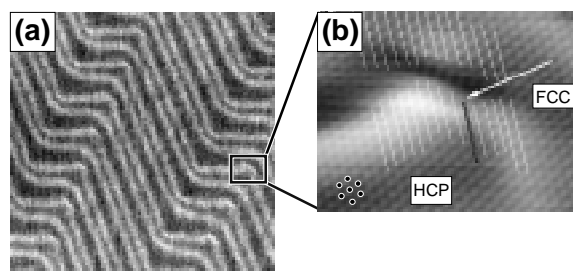


FIG. 8. Filled-state, constant-current STM images of the ($23 \times \sqrt{3}$) reconstruction on Au(111) in UHV. (a) 54 nm \times 54 nm view showing the “herringbone” pattern (0.15 V bias, 0.5 nA current, 0.02 nm height range) (Altman and Colton, 1992, reprinted with permission of Elsevier Science - NL). (b) Atomic-resolution close-up, 6.6 nm \times 5.2 nm, of the bulged herringbone corner where the transition between FCC and HCP stacking occurs (0.9 V, 0.5 nA) (Stroscio *et al.*, 1991). The approximate location of some surface atoms are marked with dots; the change in height from one to the next is about 3 pm. White lines follow rows of surface atoms across the herringbone corner, highlighting the additional row on the HCP side (indicated by the arrow).

3.1.2 Semiconductors Due to the covalent nature of the chemical bonds in a semiconductor, states within a few eV of the Fermi level tend to be more spatially localized than on metal surfaces. Therefore, atomic-resolution STM images of semiconductor surfaces can be loosely described as images of the interatomic bonds and “dangling bonds” at the surface. This localization of the electronic states leads to somewhat larger corrugations than on metals, making atomic-resolution images relatively easier to acquire on semiconductor surfaces. However, because the states may not be localized around the atom cores and may be distributed differently for filled versus empty states, determining the structure from STM images is more complicated.

The local nature of the electronic states on semiconductor surfaces is very apparent in constant current images of GaAs(110) (see GALLIUM ARSENIDE). The Ga and As atoms at the surface, which would both normally be in the surface plane, move slightly in and out of the plane in a simple (1×1) relaxation. The electronic effect of this structural relaxation, as shown in Fig. 9, is that the empty electronic states within a few volts of E_f are strongly localized on the surface Ga atoms, whereas the filled states are strongly localized on the As. The net result is that a different half of the surface atoms are seen in each image (as first reported by Feenstra *et al.*, 1987). Note that the surface shown in Fig. 9 also includes a point defect, a single missing As atom, highlighting the unique capability of STM to directly observe such structures and their affect on neighboring atoms (Lengel *et al.*, 1994).

The first surface structure ever observed with atomic resolution with an STM was the

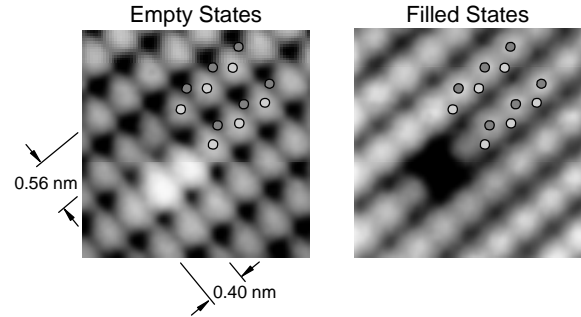


FIG. 9. Atomic-resolution empty- (2.0 V) and filled-state (1.8 V) constant-current images of the same area of a GaAs(110) surface in UHV. The location of surface Ga atoms (light circles) and As atoms (dark circles) are indicated; the height change from atom-to-atom is about 0.02 nm in the images. The defect observed is a single surface As vacancy (after Lengel *et al.*, 1994).

(7×7)-reconstructed (111) surface of silicon (Binnig *et al.*, 1983). STM images like those displayed in Fig. 10 were the critical pieces of the puzzle allowing the structure of this surface to be determined (Takayanagi *et al.*, 1985). Because constant-current images of Si(111)-(7×7) are so eye-catching (and relatively easy to acquire in UHV), they are probably the most widely displayed of all STM images and therefore warrant an explanation. Although the structure observed in the images may appear relatively simple, the actual reconstruction is quite elaborate, involving atoms in the top three layers of the surface (Fig. 10). The top-most atoms, referred to as “adatoms,” have one unfilled surface dangling bond each – the only features observed in the empty-state image. The atomic-scale features observed in the filled-state image are associated with the bonds between the adatoms and the second layer atoms, and partially-occupied dangling bonds on the second layer atoms.

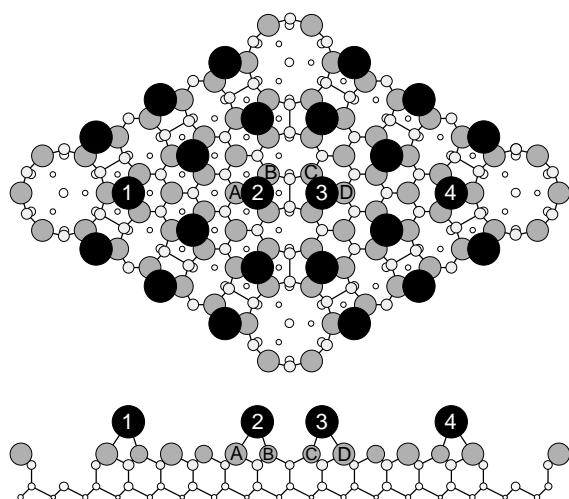
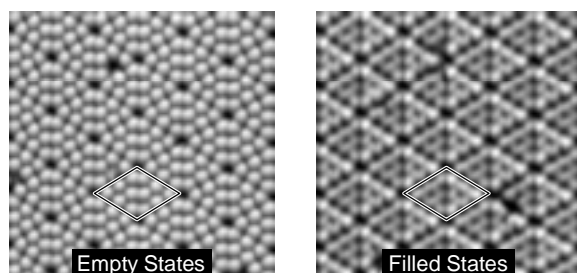


FIG. 10. The (7×7) reconstruction of Si(111) in UHV. Both empty- and filled-state constant-current images are shown ($14 \text{ nm} \times 14 \text{ nm}$, $\pm 2.0 \text{ V}$, 0.2 nm height range); one diamond-shaped (7×7) unit cell, $4.66 \text{ nm} \times 2.69 \text{ nm}$, is indicated (courtesy of A. A. Baski and the author). The structure of the unit cell is shown in top and side view (through the long diagonal) with the top-most atoms largest and darkest. Some of the atoms are labeled to aid correlation between the two views (after Takayanagi *et al.*, 1985).

3.1.3 Oxides It is well established that the catalytic properties of oxide materials depend on the structure of their surfaces, including the density and configuration of steps, point defects, and extended crystal defects that intersect the surface. Although oxide materials are generally nonconductive, sometimes surface defects or some intrinsic material property makes them conductive enough for study with STM. For example, an STM image of the (100) surface of the mixed-valence compound $\text{Mo}_{18}\text{O}_{52}$ is shown in Fig. 11 (Rohrer *et al.*, 1993). The structure of this material can be described as a stack of MoO_3 -like slabs shifted slightly

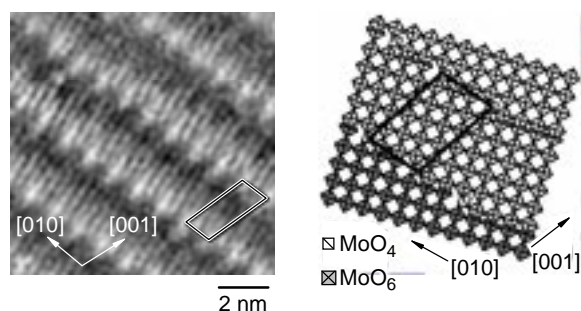


FIG. 11. Filled-state constant-current image of $\text{Mo}_{18}\text{O}_{52}(100)$ (1.6 V , 0.25 nm height range) and corresponding structural model. The planar repeat unit is indicated by the black box. The model is a polyhedral representation shaded by height (darker is lower). The sample was prepared in air and then imaged in UHV (Rohrer *et al.*, 1993, reprinted with permission of Elsevier Science - NL).

from one to the next, with the shifts referred to as crystallographic shear planes. These shear planes are observed directly in the image where they intersect the surface and create a periodic array of step-like structures. Atomic-scale structures on the surface can also be resolved, including features associated with different MoO_x polyhedral groups.

3.2 Adsorption and Film Growth

Most surface-dependent technologies depend on the chemical interaction of a surface with gaseous or liquid reactants, and/or the properties of thin films deposited on a surface. Because surface chemistry is generally heterogeneous, occurring at different rates and by different mechanisms depending on the specific local arrangements of surface atoms, the direct atom-by-atom view afforded by STM makes it a particularly effective tool for studying surface reactions and thin-film growth. By observing a surface as a function of reaction parameters, such as time, temperature, and exposure to reactants, the rates and mechanisms for the individual surface sites and reaction pathways can be studied. Note

that although STM can be used to study both atomic and molecular films, interpretation of atomic-resolution images is simpler when the types of chemical species on the surface (and their relative concentrations) are already known.

3.2.1 Atom-Resolved Surface Chemistry The ability of STM to observe surface reactions in real time is demonstrated by the series of images displayed in Fig. 12 (Besenbacher *et al.*, 1994). These frames from an STM “movie” were recorded while a Ni(110) surface at room temperature in UHV was exposed to H₂S gas. Prior to exposure, the surface was covered with oxygen, forming a (2×1) reconstruction consisting of rows of alternating Ni and O atoms; only features associated with the Ni atoms are seen in the STM image [Fig. 12(a)]. The H₂S reacts with the O atoms to form H₂O gas, leaving S behind on the surface. As O atoms are removed at the start of the reaction, the neighboring Ni atoms accumulate in small S-covered islands, creating S-covered holes nearby [Figs. 12(b)–(d)]. As the reaction proceeds, these small islands suddenly become unstable and are replaced by isolated atomic-width rows [Fig. 12(e)]. Eventually the surface becomes completely covered with such rows, forming an ordered S-induced (4×1) reconstruction, one that will not form at room temperature in the absence of O. The STM results revealed that the very small islands produced by the local removal of O create especially

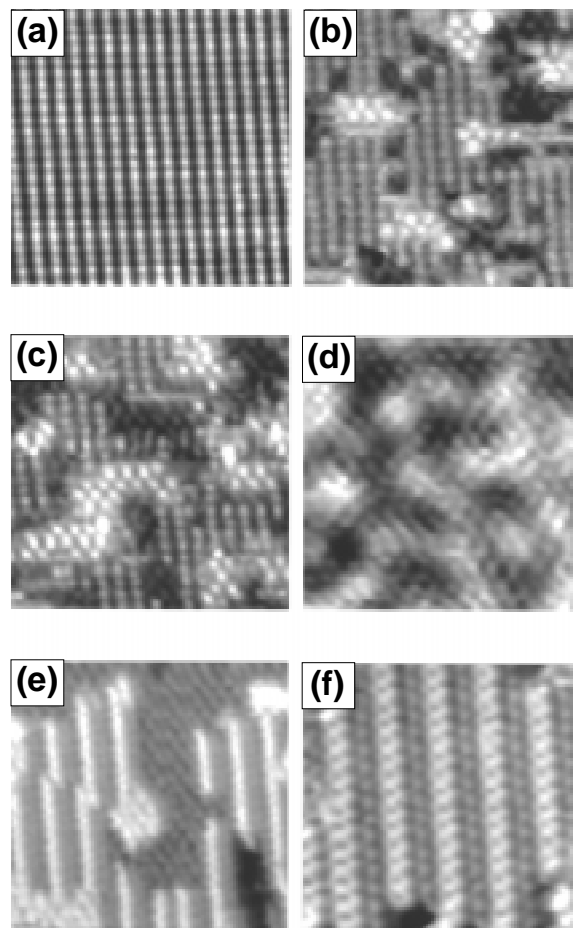


FIG. 12. Filled-state images recorded during the room-temperature reaction of H₂S with oxygen-covered Ni(110) in UHV; $\text{H}_2\text{S}_{(\text{gas})} + \text{O}_{(\text{surface})} \rightarrow \text{H}_2\text{O}_{(\text{gas})} + \text{S}_{(\text{surface})}$. (a) 0, (b) 4.0, (c) 10.6, (d) 26.6, (e) 33.3, (f) 46.6 mbar · sec. All the images are about 9.5 nm × 9.5 nm, except (f), which is 7.5 nm × 7.5 nm (Besenbacher *et al.*, 1994, reprinted with permission of the American Vacuum Society).

reactive sites for S adsorption, thereby facilitating the accumulation of S required to form the (4×1) structure.

The heterogeneous nature of surface reactions is highlighted by STM studies of the oxidation of Si(111)-(7×7), where the complex reconstruction (Fig. 10) creates a variety of inequivalent adsorption sites. As shown by the empty-state images in Fig. 13 (Martel *et al.*, 1996), when a clean Si(111) surface at room temperature is exposed to O₂ gas in UHV, the oxygen initially reacts almost exclusively with the atoms at the corners of the diamond-shaped unit cells (known as “corner hole adatoms”). The reaction results in two types of features at the corner holes, referred to as “bright” (B) and “dark” (D) sites. In addition, dark features are observed both individually and in pairs (DD). The STM images, when combined with the results of spectroscopy and other characterization techniques, revealed that the corner holes are preferred reaction sites due to their higher density of states near E_f , and that the reaction produces three types of species: an oxidized silicon

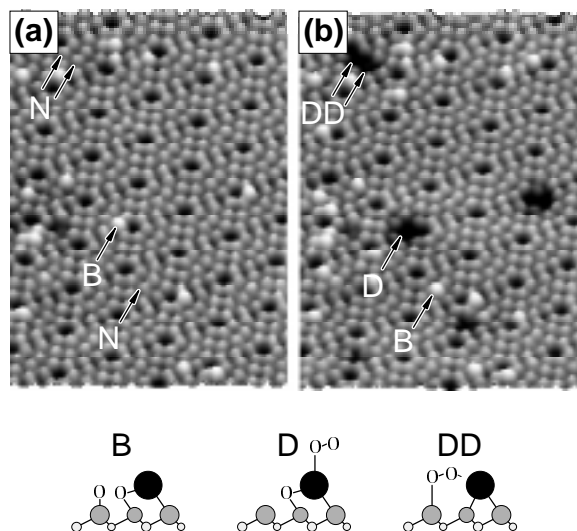


FIG. 13. Empty-state images (14 nm × 21.5 nm) of a Si(111)-(7×7) surface during the early stages of oxidation in UHV: (a) after exposure to 0.067, and (b) 0.133 mbar · sec of O₂. The arrows point to typical reaction sites: not reacted (N), bright (B), dark (D), and two adjacent dark sites (DD). Structural models for the reacted sites are also shown (after Martel *et al.*, 1996).

adatom (B), an O₂ molecule bonded to an oxidized adatom (D), and an O₂ molecule bonded to a second-layer atom and interacting with two adjacent adatoms (DD). Identification of all three species is an important step toward attaining a complete understanding of the oxidation reaction.

3.2.2 Thin-Film Morphology Just as the reaction of a surface with a gas can be followed via STM, the morphology of deposited films can be monitored during growth. Film growth involves a host of processes, including adsorption, diffusion across the surface, nucleation of islands, and sticking to island or terrace edges; studies of how the morphology depends on growth conditions elucidate these reactions. For example, in Fig. 14 the temperature-dependent film morphology observed with a variable-temperature STM is shown for a tenth of a layer of Ag deposited on Pt(111)

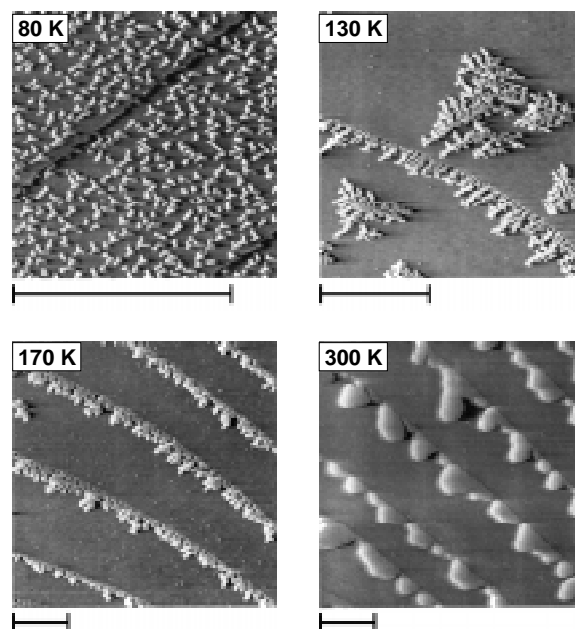


FIG. 14. Filled-state variable-temperature STM images of the growth of 0.1 layers of Ag on Pt(111) in UHV. The scale bars are all 50 nm, and the images are gray-scales of the *derivative* of the topography (which highlights edges) (Röder *et al.*, 1993, reprinted with permission of Elsevier Science - NL).

in UHV (Röder *et al.*, 1993). At 80 K the atoms migrate short distances upon deposition, forming small Y-shaped clusters (with an average of 19 atoms in each). As the temperature is increased, faster diffusion allows more of the deposited atoms to reach a Pt surface step where they become trapped, producing the morphology observed at 130 K. At this temperature migration of atoms along island edges is still hindered, however, giving the islands a jagged shape. At 170 K the temperature-dependent mobility is large enough to allow almost all nucleation to occur at step edges, which become noticeably smoother. Finally, at 300 K the film grows as round-edged islands flowing out from the step edges, close to the equilibrium morphology. These STM results, combined with other images recorded as a function of film thickness, led to a detailed understanding of the atomic-scale kinetics and mechanisms of Ag growth on Pt(111), experimentally confirming general theories about nucleation and growth (Brune *et al.*, 1994).

In addition to furthering our general understanding of growth processes, STM can be used more simply as a direct method of characterizing the nanometer-scale morphology of multilayer films. This is an important application given that many thin film-based technologies require films to be as perfect as possible for optimum performance. The type of information attainable is illustrated in Fig. 15, where an STM image of a 4 μm -thick GaSb (gallium antimonide) film grown on a GaAs(001) substrate in UHV is displayed. The film was deposited by molecular beam epitaxy (see MOLECULAR BEAM EPITAXY) for possible use in an electronic device (Thibado *et al.*, 1996). The surface consists of spiral-like mounds approximately 5 nm high, with each “step” on the surface a single atomic layer (about 0.3 nm). The

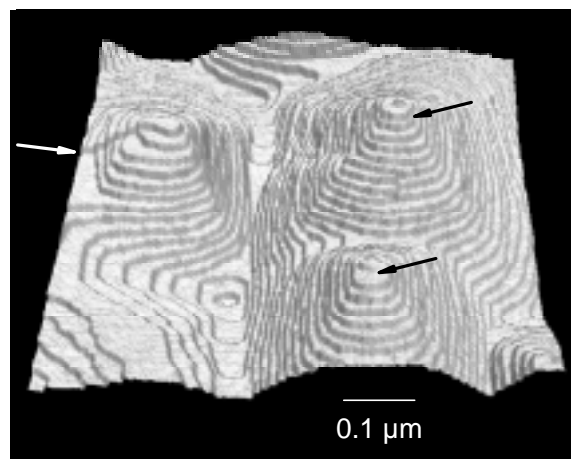


FIG. 15. The topography of a 4 μm -thick GaSb film grown on a GaAs(001) substrate by molecular beam epitaxy in UHV. Each step in the constant-current image is about 0.3 nm high. The arrows point out where threading dislocations emerge at the surface and create steps (courtesy of P. M. Thibado, B. R. Bennett, B. V. Shanabrook, and the author).

striking morphology results from the crystal lattice of GaSb being 7% larger than that of GaAs, which causes crystal dislocations to form in the deposited films. These dislocations, which are detrimental to electronic devices, thread up through the film and emerge at the surface to produce a step. This type of characterization allows the effects of various growth conditions to be directly observed, thereby simplifying the effort to improve the film quality.

3.3 Electrochemistry

Electrochemical technologies rely on processes that occur at the solid-liquid interface. Whereas in air and vacuum one can control the type and concentrations of reactants along with the substrate temperature, in an electrochemical environment an additional parameter can be varied: the electrochemical potential (see ELECTROCHEMISTRY). Control of this potential allows one to vary the thermodynamics of electrochemical reactions, including both reversible and irreversible processes such as oxidation,

reduction, deposition, and changes in surface reconstruction; STM allows the atomic-scale nature of these processes to be directly observed *in situ*. One such process is exhibited in the series of STM images in Fig. 16, recorded during the oxidation of the naturally-occurring semiconductor galena (PbS) in a solution of NaClO₄ (Higgins and Hamers, 1995). The reaction, $\text{PbS} \rightarrow \text{Pb}^{2+} + \text{S} + 2\text{e}^-$, is seen to occur almost exclusively via removal of atoms at step edges. Furthermore, impurities (I) are observed to cause etch pits (P) in the surface. Combined with STM images recorded during electrochemical reduction cycles, the complex surface electrochemistry of galena was elucidated on the atomic-scale for the first time.

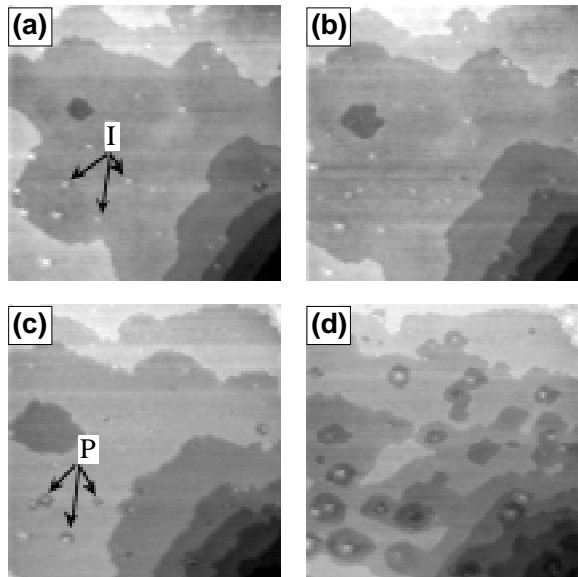


FIG. 16. A selection of constant-current images of PbS(001) acquired during electrochemical oxidation in NaClO₄. All images are 200 nm × 200 nm, with each gray level corresponding to a change in height of 0.3 nm. The images were recorded with a tunneling current of 0.17 nA, tip voltage of 0.94 V, and a sample voltage that changed from (a) 0.20 to 0.24, (b) 0.29 to 0.33, (c) 0.38 to 0.43, and (d) 0.38 to 0.34 V during image acquisition. Some surface impurities (I) and the resulting etch pits (P) are labeled (Higgins and Hamers, 1995, reprinted with permission of Elsevier Science - NL).

3.4 Surface Electronic Structure

Although some effects related to surface electronic structure were indirectly revealed in the applications discussed above, atomic-scale electronic properties can be more directly studied using the various imaging and spectroscopy modes described in Section 2. In this way the local electronic properties (including work function, conductivity, and density of states), of clean surfaces, point defects, isolated adsorbed atoms and molecules, nanometer-scale islands, and thin films can be observed. (See also ELECTRONIC STRUCTURE OF SURFACES.)

3.4.1 Conductance versus Structure One of the simplest and most direct applications of tunneling spectroscopy is the examination of the local conductance as revealed by the shape of *I-V* spectra recorded over different surface structures. A nice illustration of this application is the study of the conductance of different Cs structures observed on GaAs(110) in UHV (Whitman *et al.*, 1991). As Cs is deposited on the surface at room temperature, it first forms one-dimensional (1-D) atomic chains, then a 2-D array of planar clusters, and finally a disordered film of 3-D clusters (images not shown). As displayed in Fig. 17, *I-V* spectra recorded on clean GaAs(110) have the expected tunnel-diode shape, with zero current (and zero differential conductance) within the semiconductor bulk band gap. Spectra recorded over the Cs structures, however, show that the local “band gap” decreases as the structures change from 1- to 3-D. The 3-D structures appear metallic, i.e. there is non-zero conductance at E_f (zero sample voltage). These spectroscopy results furthered our understanding of the properties of nanometer-scale metal-on-semiconductor structures.

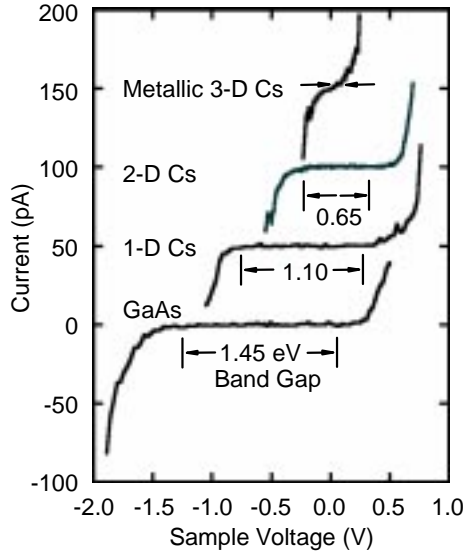


FIG. 17. Current versus voltage tunneling spectra recorded on clean and Cs-covered GaAs(110) in UHV. With increasing Cs coverage long 1-D chains, then 2-D planar clusters, and finally a disordered 3-D overlayer are observed (images not shown). The apparent “band gap” observed for each structure is indicated (Whitman *et al.*, 1991).

3.4.2 Chemically-Selective Imaging

Local variations in the density of states that are associated with particular surface atoms or molecules can sometimes be exploited to provide atom-selective topographic contrast. An extreme example is the (110) surface of GaAs discussed in Section 3.1.2 (Fig. 9), where only Ga (As) features are seen in empty (filled) states. A subtler, more elegant example is found in a study of Cr films deposited on Fe(001) (Davies *et al.*, 1996), the results of which are presented in Fig. 18. Metal “sandwiches” composed of alternating thin layers of ferromagnetic (e.g. Fe) and nonmagnetic (e.g. Cr) layers have novel magnetic properties of potential use in magnetic recording technologies. The properties are not always as expected, however, and this STM study revealed a possible cause. Rather than forming a simple overlayer, Cr alloys with the substrate, with Cr atoms randomly embedding into the surface. The Fe atoms

displaced by this process intermix with additional Cr atoms to form isolated single-layer islands. Tunneling spectra recorded over the embedded Cr atoms differ from Fe spectra, with an extra peak in the conductance about 0.3 V below E_f ; this extra conductance causes a small bump (~ 0.01 nm high) over every Cr atom in the constant-current topography recorded at negative sample bias. That spectral feature and the associated atom-selective images led directly to an understanding of the Cr/Fe interface structure.

3.5 Bulk Electronic Structure

The different chemical environment at a surface with respect to that in the bulk usually results in distinct structural and electronic properties. Exceptions to this situation occur in materials with strong covalent bonding in 2-D layers and weak non-covalent bonds holding the layers together: when the weak bonds are broken to expose a surface, the surface atoms do not differ greatly from those at the inter-layer interfaces, and STM can therefore be used to observe bulk properties. This is very

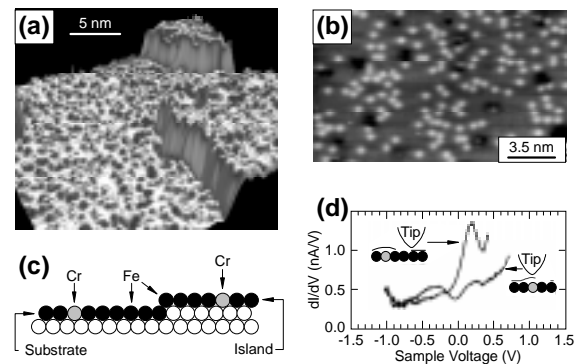


FIG. 18. (a) Filled-state image (1.1 V) of 0.4 layers of Cr deposited on Fe(100) at 290 C in UHV. Each step is 0.14 nm high and the small bumps in the topography are approximately 0.01 nm high. (b) A higher-resolution view of the Cr-induced bumps. (c) A structural model for the Cr film. The Cr atoms are embedded in the substrate, with displaced Fe atoms forming single-layer islands. (d) Conductance spectra recorded over a Cr or Fe surface atom (after Davies *et al.*, 1996).

fortuitous because the 2-D nature of such materials often gives them scientifically fascinating properties. For instance, one important class of these layered materials, transition metal dichalcogenides, exhibit both superconducting and charge density wave (CDW) phases (see COLLECTIVE PHENOMENA IN SOLIDS).

For superconducting phases, STM can be used to directly study spatial variations in the energy gap, the effect of point defects and impurities, and magnetic field effects. Because charge density waves are periodic variations of the charge density near E_f (caused by electron-phonon coupling), they can also be directly imaged with STM, as shown in Fig. 19 for TaS_2 (Liu *et al.*, 1996). On pure TaS_2 crystals the CDW is observed as a large hexagonal corrugation (0.2-0.4 nm) with a period distinctly different from the smaller corrugation (<0.1 nm) associated with the underlying crystal lattice. Bulk impurity atoms (Nb) introduce dislocations and other forms of local disorder into the CDW, but do not affect the long-range orientational order. More detailed image analysis as a function of impurity concentration showed that the CDW lattice evolves from a crystalline state to an amorphous liquid-like state with increasing concentration – a significant discovery about the nature of this material.

3.6 Atom Manipulation and Nanolithography

The nanometer-scale nature of the tip-surface interaction combined with the unprecedented degree of position control

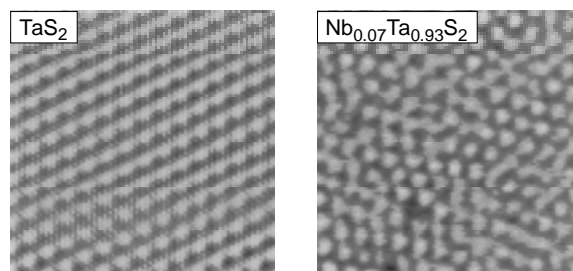


FIG. 19. Constant-current filled-state images (15 nm \times 15 nm, 50 mV, 1 nA) of $\text{Nb}_x\text{Ta}_{1-x}\text{S}_2$ crystals recorded in a nitrogen-filled glove box at 380 K ($x = 0$) and 315 K ($x = 0.07$). The large-period corrugation is due to a charge density wave that is incommensurate with the crystal lattice (the smaller, shorter-period corrugation) (Liu *et al.*, 1996, reprinted with permission of the American Vacuum Society).

available with the STM make it a revolutionary instrument for surface modification. There are four fundamental processes inherent to surface modification: removal of surface atoms, deposition of new material, lateral translation of adsorbed atoms, and induction of surface chemical reactions. All of these processes can be actuated on the atomic scale via the three basic control parameters in an STM: the tip properties, including the material composition and shape of the tip; the tunneling current; and the electric field in the tunnel junction (a function of the gap and the bias voltage). Depending on the degree of control and the intensity of the tip-surface interactions, modifications can be made from the micron to the atomic scale. Although practical applications of such “nanolithography” have yet to be realized, the STM is a new tool with which to explore the properties of nanometer-scale structures and the limits of physical lithography.

3.6.1 Electron-Stimulated Patterning

The needle-like shape of etched STM tips provides extremely effective focusing of the emitted electrons, both in tunneling and field-emission modes. Even though the total current is very small, this focusing makes the current density quite large: 10^{11} – 10^{12} times higher than a conventional electron beam with the same current. Combined with the large electric field in the tunnel junction ($\sim 10^7$ – 10^8 V/cm), that current density makes the STM an efficient tool for breaking surface chemical bonds. Fig. 20 demonstrates this phenomenon as applied to lithography on Si(001) (Lyding *et al.*, 1994), the substrate on which the semiconductor industry is based. The surface was first covered with atomic hydrogen, which reacts with the surface Si atoms, passivating their dangling bonds and making the surface unreactive to most other gases. Raising the sample bias voltage above ~ 4 V gives the electrons enough energy to break the H-Si bond and thereby locally remove H from the surface. (The H-free areas appear brighter in filled-state images due to a larger density of

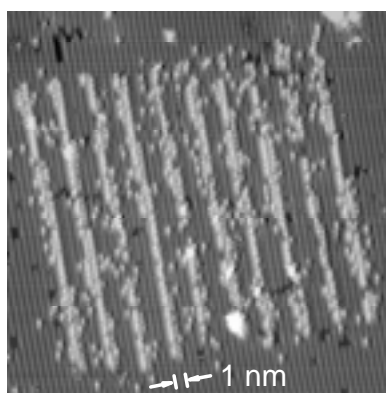


FIG. 20. Filled-state image ($37.5 \text{ nm} \times 37.5 \text{ nm}$) of nanometer-scale lithography of Si(001)-(2 \times 1) with an STM in UHV. The surface was first covered with atomic hydrogen, forming (2 \times 1)-reconstructed rows of H-Si=Si-H (the dimmer rows visible in the image). The H was then locally removed (bright rows) by scanning the desired areas with a high sample bias and current (4.5 V, 2.0 nA) (Lyding *et al.*, 1994, reprinted with permission of the American Institute of Physics). The lines are ≤ 1 nm wide on a 3 nm pitch.

states on the bare Si atoms.) This removal can be confined to lines only one or two Si atoms wide. When the patterned passivated surface is exposed to a reactant such as O_2 , only the H-free areas react (not shown).

3.6.2 Positioning Single Atoms Perhaps the most dramatic use of an STM has been to perform the ultimate surface modification: the controlled manipulation of individual surface atoms (Eigler and Schweizer, 1990). Using an STM operating in UHV at a cryogenic temperature (4 K), IBM scientists have precisely positioned adsorbed atoms by carefully placing the tip in contact with them one at a time and gently sliding them across the surface. (The atoms are otherwise immobile at this low temperature.) A sequence of images recorded during the assembly of a ring of 48 Fe atoms on

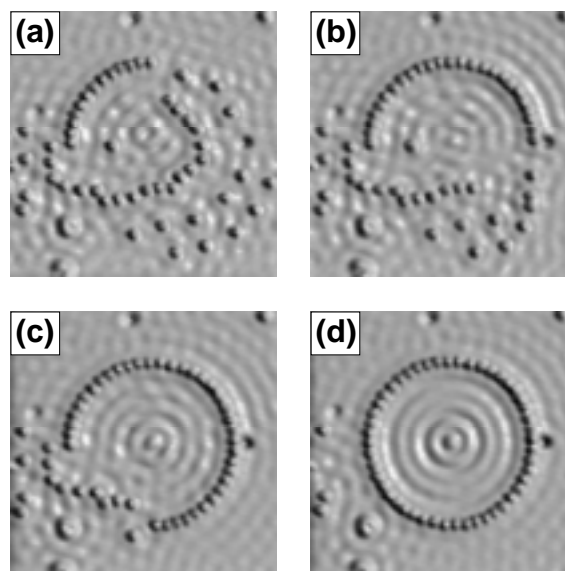


FIG. 21. (a)–(d) Sequential constant-current empty-state images (0.01 V, 1.0 nA) recorded during the assembly of a circle of Fe atoms on Cu(111) at 4 K in UHV. The average diameter of the circle is 14.25 nm. The structure was assembled one atom at a time using the STM tip. The concentric rings seen in the image are variations in the local density of states (not atomic heights) associated with standing waves created by surface electrons trapped inside the circle of Fe atoms (a “quantum corral”) (courtesy of M. F. Crommie, C. P. Lutz, and D. M. Eigler).

Cu(111) is displayed in Fig. 21. When the first image was recorded, one quarter of the ring had already been assembled and the additional Fe atoms required positioned nearby. A striking consequence of the construction of this “quantum corral” is the formation of electron standing waves within the ring, observable with the STM due to its sensitivity to charge density modulations (Crommie *et al.*, 1993). These waves are produced when surface electrons are reflected by the Fe atoms within the ring and interfere with themselves – a direct observation of the wave nature of electrons as described by quantum mechanics.

4. RELATED TECHNIQUES

The basic elements of the STM, a sharp probe held in close proximity to a sample surface with precise position control, have evolved into a remarkable number of related scanning probe microscopies capable of measuring an astonishing array of structural, electrical, and chemical properties, often with nanometer-scale spatial resolution (See, for example, Wiesendanger, 1994). Four of the most common of these techniques, all commercially available, are briefly described here.

Atomic force microscopy (AFM), the simplest extension of STM, allows the study of non-conductive samples by using the force of the tip-surface interaction as the control parameter. In an AFM the tip usually consists of a micron-sized silicon nitride pyramid on the end of a few hundred micron-long silicon nitride microcantilever, fabricated using semiconductor lithography and etching techniques. By maintaining a constant tip-surface force (as measured by the deflection of the cantilever and typically in the range of 10^{-8} to 10^{-9} N), the tip can be rastered across a surface to routinely observe topography with ~ 1 nm resolution. Moreover, a variety of imaging and

spectroscopy modes have been developed to measure force-related phenomena, including friction, adhesion, and indentation. In addition to being a powerful research tool, AFM is widely used for routine high-resolution microscopy due to its ability to image almost any type of material under ambient conditions.

In magnetic force microscopy (MFM) the spatial variation of the magnetic force interaction between a magnetic tip and sample is measured, usually by mounting a magnetic tip on the end of an AFM-style cantilever. In this way, images of the stray magnetic field (or its gradient) above a surface can be acquired with a spatial resolution of 20 to 100 nm. Because MFM works under ambient conditions and on samples with nonmagnetic coatings or surface contamination, it is particularly useful for characterizing magnetic recording media.

Near-field scanning optical microscopy (NSOM) or scanning near-field optical microscopy (SNOM) replaces the STM tip with an optical fiber drawn to a point of ~ 100 nm diameter. The fiber is coated with metal everywhere but on the end, thereby defining a nanometer-scale aperture that is held ~ 10 nm from the sample. The evanescent light either reflected from or transmitted through a sample is then collected with high spatial resolution. Whereas the resolution of conventional optics is limited by diffraction, collecting the light in this “near-field” regime enables a spatial resolution much less than the wavelength of the light. In addition to providing high-resolution optical microscopy, spectroscopy can be performed on the collected light allowing the optical characterization of material defects, nanometer-scale structures, and molecular properties (via fluorescence detection).

Ballistic electron emission microscopy (BEEM) was developed in order to characterize electron transport through buried interfaces, typically between a thin film and a substrate with different electrical properties (e.g. a metal film on a semiconductor). Whereas STM is a two-electrode technique (the tip and the sample), BEEM adds a third electrode, a current collector on the edge of the thin film. The tip injects electrons into the thin film, almost all of which reach the buried interface without energy loss. Current observed at the collector is therefore a measure of electron scattering at the interface; it can be recorded as a function of the tip position along with an STM image, providing a simultaneous image of the buried interface. Furthermore, by measuring the dependence of the collector current on the sample bias, spectroscopy of interface electronic transport can also be performed.

ACKNOWLEDGEMENTS

Preparation of this article and the authors work described herein were supported by the Office of Naval Research.

GLOSSARY

Adsorption: The process whereby an atom or molecule becomes bonded to a surface.

Dangling Bond: An unbonded molecular orbital on a surface atom of a covalent or ionic crystal.

Density of States: The number of electronic levels per unit energy in a material.

Fermi Level (E_f): The energy of the highest occupied electronic state in a material at 0 K.

Miller Indices: Notation (hkl) used to describe a surface of a crystal. For a cubic crystal, the indices define a vector perpendicular to the surface, $h\hat{x} + k\hat{y} + l\hat{z}$, where \hat{x} , \hat{y} , and \hat{z} are the crystal axes.

Piezoelectric Ceramic: A material that expands or contracts when an electric field is applied across it. (See PIEZOELECTRIC DEVICES.)

Reconstruction: A rearrangement of the atoms on a crystal surface that changes their symmetry with respect to bulk positions. When the rearrangement is periodic it is denoted by the size of the unit cell, ($m \times n$), with respect to the natural crystal structure, (1×1).

Surface Science: The study of the structural, electronic, and chemical properties of surfaces, interfaces, and thin films. (see AUGER SPECTROSCOPY, CATALYSIS, CHARACTERIZATION AND ANALYSIS OF MATERIALS, CVD, ELECTRON DIFFRACTION, ELECTRON MICROSCOPY, ELECTRONIC STRUCTURE OF SURFACES, FIELD ION MICROSCOPY, MOLECULAR BEAM EPITAXY, and PHOTOEMISSION AND PHOTOELECTRON SPECTRA.)

Surface Step: The place on a crystal surface where the height changes by one or more discrete layers of atoms.

Tunneling: The quantum-mechanical process whereby an electron is transported across a classically-forbidden energy barrier.

Ultra-high Vacuum (UHV): A pressure $< 1 \times 10^{-7}$ Pa, low enough to prevent contamination of a surface by residual gases for many minutes.

Unit Cell: The periodic structural unit on a crystal surface.

Work Function: The energy required to move an electron at the Fermi level from the surface into the vacuum. (See ELECTRONIC STRUCTURE OF SURFACES.)

List of Works Cited

- Altman, E. I., Colton, R. J. (1992), Surf. Sci. 279, 49-67.
- Besenbacher, F., Laegsgaard, E., Nielsen, L. Pleth, Ruan, L., Stensgaard, I. (1994), J. Vac. Sci. Technol. B 12, 1758-1763.
- Binnig, G., Rohrer, H., Gerber, Ch., Weibel, E. (1982a), Appl. Phys. Lett. 40, 178-180.
- Binnig, G., Rohrer, H., Gerber, Ch., Weibel, E. (1982b), Physica 109-110B+C, 2075-2077.
- Binnig, G., Rohrer, H., Gerber, Ch., Weibel, E. (1983), Phys. Rev. Lett. 50, 120-123.
- Binnig, G., Smith, D. P. E. (1986), Rev. Sci. Instrum. 57, 1688-1689.
- Brune, H., Röder, H., Boragno, C., Kern, K. (1994), Phys. Rev. Lett. 73, 1955-1958.
- Crommie, M. F., Lutz, C. P., Eigler, D. M. (1993), Science 262, 218-220.
- Davies, A., Stroscio, J. A., Pierce, D. T., Celotta, R. J. (1996), Phys. Rev. Lett. 76, 4175-4178.
- Eigler, D. M., Schweizer, E. K. (1990), Nature 344, 524-526.
- Feenstra, R. M., Stroscio, J. A., Tersoff, J., Fein, A. P. (1987), Phys. Rev. Lett. 58, 1192-1195.
- Higgins, S. R., Hamers, R. J. (1995), Surf. Sci. 324, 263-281.
- Lengel, G., Wilkins, R., Brown, G., Weimer, M., Gryko, J., Allen, R. E. (1994), Phys. Rev. Lett. 72, 836-839.
- Liu, J., Huang, J.-L., Lieber, C. M. (1996), J. Vac. Sci. Technol. B 14, 1064-1069.
- Lyding, J. W., Shen, T.-C., Hubacek, J. S., Tucker, J. R., Abeln, G. C. (1994), Appl. Phys. Lett. 64, 2010-2012.
- Martel, R., Avouris, Ph., Lyo, I.-W. (1996), Science 272, 385-388.
- Röder, H., Brune, H., Bucher, J., Kern, K. (1993), Surf. Sci. 298, 121-126.
- Rohrer, G. S., Lu, W., Smith, R. L., Hutchinson, A. (1993), Surf. Sci. 292, 261-266.
- Stroscio, J. A., Pierce, D. T., Dragoset, R. A., First, P. N. (1991), J. Vac. Sci. Technol. A 10, 1981-1985.
- Takayanagi, K., Tanishiro, Y., Takahashi, M., Takahashi, S. (1985), J. Vac. Sci. Technol. A 3, 1502-1510.
- Thibado, P. M., Bennett, B. R., Twigg, M. E., Shanabrook, B. V., Whitman, L. J. (1996), J. Vac. Sci. Technol. A 14, 885-889.
- Whitman, L. J., Stroscio, J. A., Dragoset, R. A., Celotta, R. J. (1991), Phys. Rev. Lett. 66, 1338-1341.
- Wiesendanger, R. (1994). Scanning Probe Microscopy and Spectroscopy. Cambridge, Cambridge University Press.
- Wöll, Ch., Chiang, S., Wilson, R.J., Lippel, P.H. (1989), Phys. Rev. B 39, 7988-7991.
- Young, R., Ward, J., Scire, F. (1972), Rev. Sci. Instrum. 43, 999-1011.

Further Reading

Binnig, G. , Rohrer, H. (1987), Rev. Mod. Phys. 59, 615–625.

Bonnell, D. A. (Eds.) (1993), Scanning Tunneling Microscopy and Spectroscopy: Theory, Techniques, and Applications, New York: VCH.

DiNardo, N. J. (1994), Nanoscale Characterization of Surfaces and Interfaces, New York: VCH.

Duke, C. (Ed.) (1994), Surface Science: The First Thirty Years, Surf. Sci. 299/300, 1–1054.

Güntherodt, H.-J., Wiesendanger, R. (1994), Scanning Tunneling Microscopy I: General Principles and Applications to Clean and Adsorbate-Covered Surfaces, 2nd ed., Springer Series in Surface Sciences, Vol. 20. Berlin: Springer-Verlag.

Kubby, J. A., Boland, J. J. (1996), Scanning Tunneling Microscopy of Semiconductor Surfaces, Surf. Sci. Rep. 26, 61–204.

Kuk, Y., Silverman, P. J., (1989), Rev. Sci. Instrum. 60, 165–180.

Magonov, S. N. (1996), Surface Analysis With STM and AFM : Experimental and Theoretical Aspects of Image Analysis, Weinheim: VCH.

Stroscio, J. A., Kaiser, W. J. (Eds.) (1993), Scanning Tunneling Microscopy, Boston: Academic.

Wiesendanger, R., Güntherodt, H.-J. (1995), Scanning Tunneling Microscopy II: Further Applications and Related Scanning Techniques, 2nd ed., Springer Series in Surface Sciences, Vol. 28. Berlin: Springer-Verlag.

Wiesendanger, R., Güntherodt, H.-J. (1996), Scanning Tunneling Microscopy III: Theory of STM and Related Scanning Probe Methods, 2nd ed., Springer Series in Surface Sciences, Vol. 29. Berlin: Springer-Verlag.

Zangwill, A. (1988), Physics at Surfaces, Cambridge: Cambridge University Press.